Best Practices for Steady-State $scCO_2$–Brine Relative Permeability Measurements

Naser Ansaribaranghar[1], *Hamidreza* Shahosseini[1], *Mahsan* Basafa[1], *Maziyar* Mahmoodi[1], *Yueping* Yu[1], *Alejandro* Romero Fragoso[1], *Lucky* Abiashue[1], *and Lesley A.* James[1,*]

[1]Department of Process Engineering, Faculty of Engineering and Applied Science, Memorial University, St. John's, NL, A1C 5S7, Canada

Abstract. Accurate steady-state supercritical CO_2 ($scCO_2$)–brine relative permeability (k_r) data is essential for reliable CCUS storage studies, but obtaining high-quality experimental measurements and converting them into dependable k_r curves presents significant challenges. We present a comprehensive best-practice workflow for generating reliable steady-state k_r in $scCO_2$–brine systems utilizing a closed-loop high-pressure, high-temperature (HPHT) architecture. Unlike much of the existing steady-state gas–brine k_r literature, which often reports only a subset of critical QC steps or compares datasets generated with different equipment and saturation-history designs, this work consolidates a complete HPHT workflow. We provide detailed guidance on all aspects of steady-state $scCO_2$–brine coreflooding, including: core handling and preparation; porosity and absolute permeability measurement; leak detection and system volume calibration; CO_2 and brine conditioning and equilibration; fluid-property measurement; maintaining pressure–temperature stability; designing fractional-flow sequences to achieve near-equal saturation spacing; selecting appropriate flow rates; correcting pressure tare/zero-offset for ΔP measurements; performing multi-rate checks to identify and correct capillary end effects; configuring ΔP taps/measurements and selecting transducers; choosing and tuning backpressure regulators; and operating and calibrating separators. We demonstrate the workflow through drainage → imbibition → secondary drainage cycles to evaluate hysteresis and repeatability, applying rigorous steady-state acceptance criteria based on simultaneous stabilization of differential pressure, phase flow rates, and separator-derived saturation trends. We also present an uncertainty framework that accounts for errors in differential pressure, rate measurements, fluid properties, and separator-level volume readings, allowing these uncertainties to be propagated into the final k_r values. This workflow enhances reproducibility and ensures that steady-state $scCO_2$–brine k_r data is ready for direct use in CCUS simulators.

1 Introduction

1.1 The importance of relative permeability (k_r) and capillary pressure (P_c) in carbon capture, utilization, and storage (CCUS)

The geological storage of CO_2 in deep saline formations is a primary mechanism for mitigating anthropogenic greenhouse gas emissions. Successful CCUS implementation relies on accurate characterization of multiphase flow in reservoir rock [1,2]. In particular, steady-state relative permeability (k_r) and capillary pressure (P_c) curves for the $scCO_2$–brine system govern CO_2 injectivity, plume migration, residual trapping efficiency, and long-term storage security [3–6]. These parameters are critical inputs for reservoir simulation and directly influence predicted plume footprint [4,7,8].

While both steady-state and unsteady-state methods are used to measure k_r, the steady-state method is strongly preferred for $scCO_2$–brine systems. The low viscosity and high density of $scCO_2$ create adverse mobility ratios and strong buoyancy effects that often cause viscous fingering and early breakthrough in unsteady-state tests. Steady-state co-injection avoids these transient instabilities by allowing thermodynamic and saturation equilibrium to be reached at each fractional flow step [10–12].

1.2 Literature review: methodological and physical inconsistencies in $scCO_2$–brine systems

Despite the clear need for high-quality $scCO_2$–brine multiphase flow data, the existing special core analysis (SCAL) literature shows considerable scatter in $scCO_2$-brine relative permeability and residual trapping. Much of this variability is driven by methodological inconsistencies, specifically regarding Capillary End Effects (CEE) and thermodynamic fluid equilibration times, which obscure intrinsic rock properties. Differences in methodological choices regarding flow-rate dependency and experimental artifacts make direct cross-study comparisons challenging.

* Corresponding author: ljames@mun.ca

1.2.1 Capillary end effects (CEE) and measurements

A primary challenge is the Capillary End Effect (CEE), where the wetting phase accumulates at the core outlet. Because $scCO_2$ has a very low viscosity, capillary forces can represent up to 20% of the total pressure drop across standard core plugs, severely underestimating the CO_2 relative permeability and distorting saturation profiles [13,14].

Benson et al. review macroscopic two-phase flow concepts, capillary-dominated regimes, and extensions of Darcy's law in porous media [15]. Researchers employ vastly different techniques to mitigate CEE. Physical mitigation strategies include utilizing exceptionally long cores (up to 60 cm) equipped with internal pressure taps to isolate a uniform saturation zone free of end effects [13]. Mathematical mitigation involves multi-rate bump tests alongside analytical techniques like the Intercept Method (originally proposed by Virnovsky et al. [16] and later presented by Gupta and Maloney [14]) to extrapolate true relative permeability. Furthermore, the application of In-Situ Saturation Monitoring (ISSM) varies widely. Researchers like Krause et al., Krevor et al., and Pini et al. heavily utilized medical X-ray CT scanners to map 3D saturation gradients, whereas others achieve accurate results using high-precision acoustic separators combined with rigorous mass balance [1,11,17,18].

1.2.2 Fluid equilibration and mass transfer artifacts

Finally, a critical discrepancy in the literature lies in thermodynamic fluid equilibration times and the management of mutual solubility. The $scCO_2$–brine system is characterized by significant mutual solubility; water evaporates into the $scCO_2$ stream while CO_2 dissolves into the aqueous phase. Miri and Hellevang and Berrezueta et al. review the consequences of fluid–rock interactions and salt precipitation in CO_2 storage [19,20].

If experimental fluids are not properly pre-equilibrated, continuous mass transfer within the core leads to the artificial dissolution of trapped CO_2 and the evaporation of connate water [21]. This "drying effect" can induce localized salt precipitation, altering the rock's pore structure and reducing absolute permeability, a phenomenon also observed at the field scale in the Ketzin pilot project [22,23]. While some studies ensure extensive equilibration (such as Mascle et al. utilizing 168 to 504 hours, and Richardson et al. using over 336 hours) others report shorter times [24], leading to compositional artifacts that mask the true multiphase flow physics [17,24,25].

1.2.3 Existing methodological guidelines and gaps

The inconsistencies in $scCO_2$–brine data indicate a need for standardized laboratory protocols [26,27]. Similarly, Burnside & Naylor reviewed the important implications of relative permeability on residual trapping, emphasizing the significant consequences of experimental scatter on storage capacity predictions [3]. While these early papers identified macroscopic problems (such as core heterogeneity, capillary end effects, and gravity segregation), they provided general, high-level recommendations rather than specific, step-by-step engineering execution.

Targeted research reports, such as the comprehensive overview by Krause et al., deeply analyzed the physical and theoretical issues affecting data reliability in CCUS relative permeabilities [28]. However, there is a gap in translating these fundamental flow issues into a rigorous quality-control checklist and a physical equipment design. In traditional oil and gas Special Core Analysis (SCAL), McPhee et al. is a standard reference for laboratory core analysis procedures [29]. Yet, conventional SCAL guides focus heavily on oil-brine systems and do not adequately address the unique "liquid-like density and gas-like viscosity" duality, adverse mobility ratios, and mutual solubility (drying effects) inherent to $scCO_2$–brine displacements.

More recently, there has been a push to reconcile different experimental methods and ensure data is ready for reservoir simulation. Mascle et al. [31] measured CO_2–brine relative permeability by steady-state and unsteady-state methods on a homogeneous Fontainebleau sandstone. The present workflow differs in its closed-loop recirculating HPHT architecture, which keeps the fluids mutually saturated throughout the coreflood, suppressing drying and exsolution artifacts rather than relying on batch pre-equilibration.

1.3 Objectives and workflow

To address the lack of practical guidelines, our objective is to provide a structured and practical workflow to conduct steady-state $scCO_2$–brine relative permeability measurements using a closed-loop HPHT system. The full $scCO_2$–brine relative permeability datasets generated with this workflow are reported in a companion paper (SCA2026-071); the present paper documents the measurement workflow itself. While existing literature shares the overarching goal of improving data quality for CCUS, this work provides a detailed, hardware-focused workflow with four key contributions:

Closed-loop HPHT system: The precise recirculating closed-loop system required to physically maintain continuous phase equilibrium and prevent mass-transfer artifacts dynamically throughout the coreflood is detailed. This is in contrast to guidelines that merely suggest fluid equilibration.

Rigorous steady-state acceptance criteria: Strict, simultaneous acceptance criteria based on the stabilization of differential pressure, phase flow rates, and separator-derived saturation trends are explained. This goes beyond subjective visual observations of steady state.

Mathematical capillary end effect (CEE) mitigation: Analytical techniques such as the Intercept Method incorporated into multi-rate bump-test procedures mathematically correct for capillary end effects (up to 20% of the total pressure drop) that uniquely affect low-viscosity $scCO_2$ displacements.

Absolute propagated uncertainty framework: A quantitative framework is detailed that systematically accounts for compounding errors in differential pressure, flow rates, fluid properties, and separator-level volume readings, allowing these uncertainties to be propagated into the final relative permeability values.

This workflow is organized into five main stages, providing a complete methodology to design, executing, and validate steady-state $scCO_2$–brine relative permeability experiments under HPHT conditions:

Pre-experimental analysis and preparation: Establish consistent initial conditions through core preparation, brine formulation, and the rigorous characterization of rock, fluids, and core–fluid interactions.

Closed-loop HPHT system setup and conditioning: Define the experimental recirculating system, verify its pressure integrity, determine internal dead volumes, and establish the injection strategy and required measurement parameters.

Saturation and relative permeability determination: Develop the framework for calculating core saturation and relative permeability based on steady-state flow conditions and material balance.

Uncertainty analysis of measurements: Quantify the impact of instrumental and measurement uncertainties on phase saturation and relative permeability using an absolute propagated uncertainty approach, ensuring simulation readiness.

Post-experimental measurements and analysis: Validate experimental results through final mass balance verification, reassessment of core properties, and the evaluation of porosity–permeability changes and recovery after cleaning.

2 Materials and methods

2.1 Pre-experimental analysis and preparation for steady-state $scCO_2$–brine relative permeability measurements

2.1.1 Core and CO_2-saturated (live) brine preparation

Prior to conducting steady-state $scCO_2$–brine relative permeability experiments, it is essential to establish consistent and well-defined initial conditions. This is achieved through (*i*) preparation of core samples and $scCO_2$-saturated (live) brine and (*ii*) pre-experimental analyses of rock, fluids, and rock–fluid interactions (including porosity, permeability, fluid thermophysical properties, and interaction parameters such as wettability and interfacial tension).

The preparation stage ensures that the core and fluids are clean, stable, and representative, while the characterization stage provides the key input parameters required for the design and interpretation of the experiments.

Preparation of core sample

Core sample preparation is performed before core characterization (porosity, permeability, X-ray diffraction (XRD), and CT scan) and relative permeability testing to ensure that the rock is clean, physically consistent, and representative of the porous medium. This preparation includes core end trimming, core cleaning and drying.

Preparation of dead brine and CO_2-saturated (live) brine

Dead brine was synthesized using deionized water and analytical-grade salts to match target reservoir salinity, and the final composition was verified via total dissolved solids (TDS) measurements.

Live brine was prepared by charging dead brine and excess CO_2 into a heated accumulator at experimental conditions (77 °C, 4350 psi). The mixture was continuously agitated until thermodynamic equilibrium was achieved, after which excess free CO_2 was vented through a back pressure regulator to ensure a single-phase saturated solution. At these conditions the CO_2 is in its supercritical state.

For reactive carbonate lithologies such as dolomite, an additional rock-specific pre-equilibration step is required to eliminate fluid–rock geochemical artifacts (dissolution or precipitation) that would otherwise distort relative permeability measurements. Geochemical modeling using PHREEQC (Thermoddem v1.10 database) is recommended to determine the equilibrium brine composition and minimum pre-equilibration time or pore volumes via batch kinetic and 1D reactive-transport simulations, ensuring the dolomite saturation index remains near zero throughout the test. The detailed protocol, including kinetic rate parameters and Damköhler-number analysis, is available from the authors upon request or as supplementary material. This step has not previously been addressed in the steady-state $scCO_2$–brine literature for carbonate systems.

2.1.2 Characterizing the core, brine (dead and live), $scCO_2$, and core–brine interactions.

Routine core properties (gas porosity, Klinkenberg-corrected permeability, XRD mineralogy, and CT morphology) and HPHT fluid properties (density and viscosity of dead brine, live brine, and $scCO_2$) were measured using standard laboratory apparatuses. Core, fluid, and core–fluid interaction properties were characterized using standard laboratory techniques prior to relative permeability testing. For the core samples, absolute permeability was determined from steady-state gas flow measurements with Klinkenberg correction. Porosity was obtained via gas expansion (Boyle's law). Internal morphology and heterogeneity were assessed non-destructively by X-ray computed tomography (CT) scanning. Quantitative mineralogy, with emphasis on reactive carbonate phases, was determined by X-ray diffraction (XRD) with Rietveld refinement. Fluid properties under HPHT conditions, including density and viscosity of dead brine, CO_2-saturated live brine, and $scCO_2$, were measured with high-pressure densitometry and viscometry; these properties were also monitored during experiments to confirm stability. Core–fluid interactions could be characterized at full reservoir

conditions (77 °C, 4350 psi) by interfacial tension measurements using axisymmetric drop shape analysis and by contact angle measurements on representative rock surfaces to establish wettability relevant to the $scCO_2$–brine system. The interfacial-tension and contact-angle measurements can be carried out at the same supercritical reservoir conditions as the corefloods (77 °C and 4350 psi), so that the resulting wettability and IFT values correspond to the $scCO_2$–brine system rather than to gaseous CO_2.

Core characterization

Core permeability: A reliable estimate of permeability is required prior to relative permeability experiments to screen core quality, establish a baseline, and support the design of flow conditions. Gas permeability is used for this purpose because it is fast, clean, and not affected by fluid–rock interactions.

Core porosity: A reliable estimate of core porosity is required to quantify the pore volume available for fluid storage and flow, and to support the interpretation of relative permeability results.

Core morphology: The pore structure and internal heterogeneity of the core samples were evaluated using X-ray computed tomography (CT) scanning. This non-destructive imaging technique provides high-resolution three-dimensional images of the pore network, enabling quantitative assessment of porosity distribution, pore-size distribution, presence of fractures or vugs, and overall sample homogeneity. Such morphological characterization is essential for interpreting relative permeability results and for identifying potential experimental artifacts associated with core heterogeneity. CT scans were performed on the trimmed, clean, and dry core samples prior to relative permeability testing.

Core Mineralogy X-ray diffraction (XRD) analysis was conducted to determine the quantitative mineralogical composition of the core samples. Powdered subsamples were analyzed using a standard XRD diffractometer, and mineral phases were identified and quantified using the Rietveld refinement method. Accurate mineralogical characterization is critical for understanding potential fluid–rock interactions (particularly in reactive carbonate lithologies such as dolomite) and for interpreting any post-experiment changes in porosity and permeability. Particular attention was paid to Fe-bearing carbonates such as siderite and to calcite, because dissolution–reprecipitation upon contact with $scCO_2$–acidified brine can drive localized pore plugging and measurable permeability reduction [38].

Brine (live/dead), $scCO_2$ characterization

Density and viscosity measurement under HPHT conditions Accurate fluid properties are required prior to relative permeability experiments, as density and viscosity directly affect mass balance, pressure drop, and mobility calculations. In CO_2–brine systems, these properties change after gas dissolution; therefore, the properties of dead brine, CO_2-saturated (live) brine, and $scCO_2$ were determined under representative pressure and temperature conditions. In addition to pre-experimental measurements, density and viscosity can also be monitored during relative permeability tests to verify the stability of fluid properties.

2.1.3 Core saturation and loading

Dried cores were vacuum-saturated with dead brine and loaded into a hydrostatic core holder. To mitigate gravity override and fluid segregation driven by the $scCO_2$–brine density contrast, the core holder was oriented vertically to enable top-to-bottom co-injection. System sealing integrity was rigorously verified via N_2 and silicone oil leakage tests at target confining pressures prior to loop integration.

2.2 Closed-loop HPHT setup for steady-state $scCO_2$–brine relative permeability testing

Fig. 1 presents the process and instrumentation diagram (P&ID) of the closed-loop high-pressure high-temperature (HPHT) system used for steady-state $scCO_2$–brine relative permeability measurements at the Hibernia Enhanced Oil Recovery (EOR) Laboratory, Memorial University, Canada. The system is installed inside a forced convection oven to simulate reservoir temperature conditions and maintain a uniform temperature distribution across the setup.

To provide a clear understanding of the system configuration and its operational roles, the HPHT setup is organized into key functional subsystems, as summarized in Table 1. The recirculating closed-loop arrangement adopted here builds on the configuration first introduced by Guo and Vatne [34].

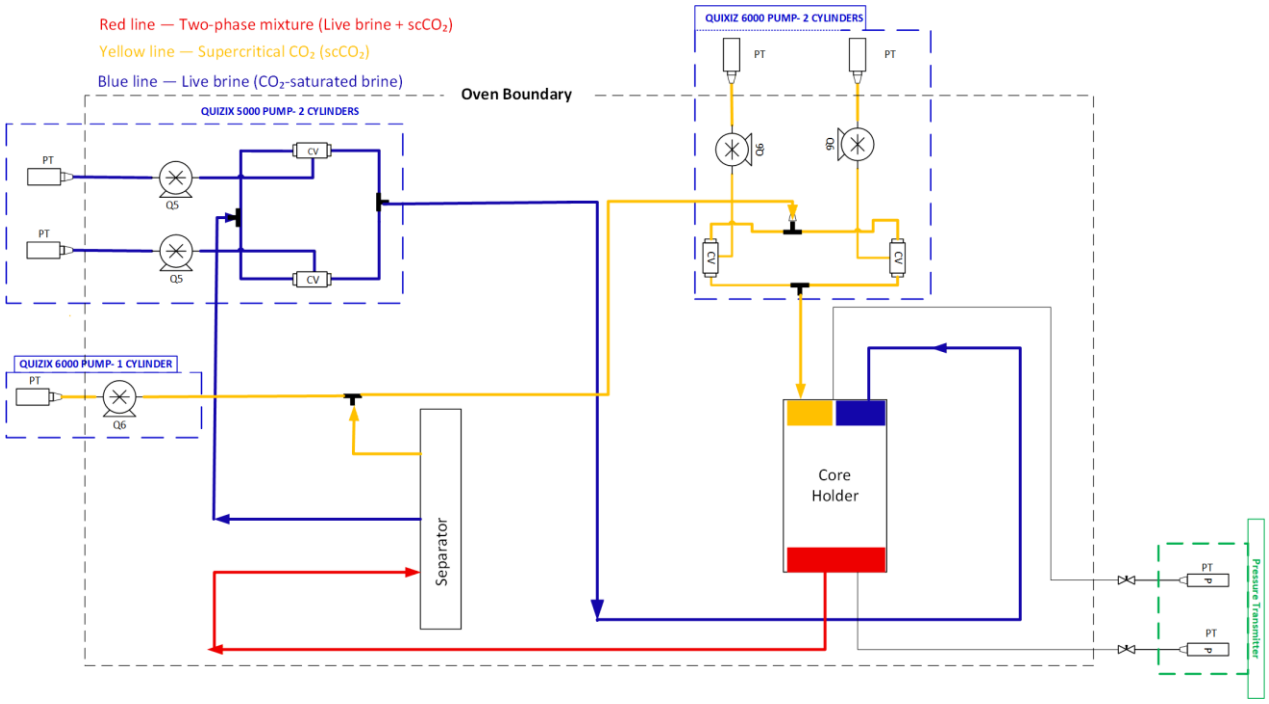

Fig. 1. P&ID of the closed-loop HPHT system for steady-state CO_2–brine relative permeability testing. The diagram has been simplified to show the major subsystems and the principal flow paths, with individual valve and fitting tags omitted, to improve readability.

Table 1. Subsystem classification of the closed-loop HPHT system for CO_2–brine relative permeability testing.

Subsystem	Main components	Function
Temperature Control System- Oven / Heating System (Provider: Despatch Industries) (highlighted by the black rectangular area in P&ID)	Despatch RAF Series forced convection oven with recirculating airflow, electric heating elements, and digital temperature controller	Provides uniform and controlled temperature using forced convection and recirculating airflow, ensuring stable thermal conditions for the entire system under HPHT operation.
Fluid injection and pressurizing system (Provider: AMETEK Chandler Engineering system) (highlighted by the blue rectangular area in P&ID)	1- Quizix® C-5000 Series High-Pressure Pump (two-cylinder) with CV-310 air-actuated three-way valves	Provides continuous and stable brine injection at controlled flow rate and pressure
	2- Quizix® C-6000 Series High-Pressure Pump (two-cylinder) with CV-510 air-actuated three-way valves	Provides continuous injection of CO_2 (gas phase) at high pressure with precise flow and pressure control
	3- Quizix® C-6000 Series High-Pressure Pump (single-cylinder)	Used for servo pressure compensation, maintaining system pressure by compensating for gas leakage and probable CO_2 dissolution during live brine preparation and operation
	4- Quizix® QX-20000 Series High-Pressure Pump (two-cylinder) with CV-520 air-actuated three-way valves	Supplies silicone oil for accumulator pressurization and overburden pressure, simulating reservoir stress conditions
Separation system (Provider: New England Research, Inc. (NER)) (highlighted by the light blue rectangular area in P&ID)	2-phase separator equipped with Acoustic Level Detection Module (ALDM) and ultrasonic transducers (SEP-*)	Separates CO_2/brine phases by removing excess free CO_2 beyond solubility limits while maintaining CO_2-saturated brine for recirculation. Supports closed-loop operation and provides real-time phase level measurements under HPHT conditions.
Core Holder & Confinement System (Provider: Vinci Technologies)	HYC-series Hydrostatic Core Holder (CH-*)	Provides a sealed and mechanically stable environment for the core sample, enabling confining pressure application and controlled fluid flow under externally controlled temperature conditions
Measurement and instrumentation system	1- Intelligent Pressure Transmitters	Provides accurate and continuous measurement of pressure throughout

(highlighted by the green rectangular area in P&ID) (Provider: Paroscientific Digiquartz®- New England Research (NER))	(Series 6000) (PT-*)	the system, enabling real-time monitoring, control, and reliable data acquisition under HP conditions.
	2- Mechanical pressure gauges (PG-*)	Provides local visual indication of accumulator pressure for quick monitoring and operational safety.
	3- Acoustic Level Detection Module (ALDM) with ultrasonic transducers	Measures fluid interface levels inside the separator and calculates absolute and relative volumes of light and heavy phases under HPHT conditions.
Fluid property measurement system (highlighted by the purple rectangular area in P&ID)	1- Densitometer (Anton Paar mPDS 5) 2- HyperVisc PVT Viscometer (Hydramotion)	Measures fluid properties during the relative permeability test to ensure consistent fluid behavior and to monitor the impact of mineral dissolution on fluid properties, permeability, and porosity.
Flow Network System (Lines + Valves + Fittings) (Provider: Autoclave Engineers)	1- Tubing and pipelines 2- Needle valves (2V-*) 3- Ball valves (SV-*) 4- 3-way valves / manifolds (MV-*) 5- Constant volume valves (VV-*) 6- Tees (TE-*), *unions (UN-*)*, adapters (AA-*) 7- Cross and elbow fittings (CE-*, *EL-**)	Provides controlled routing, distribution, and isolation of fluids throughout the system, ensuring safe and stable flow under HPHT conditions.
Accumulator cylinders (fluid storage system) (highlighted by the red rectangular area in P&ID)	1- Dead brine accumulator cylinder (A-202) 2- CO_2 (gas) accumulator cylinder (A-204) 3- Gas–brine accumulator cylinder (A-203)	Provides storage and a stable pressurized supply of CO_2, live brine, and dead brine to enable continuous and controlled injection under HPHT conditions.
Safety & Protection System (Provider: Swagelok and OsecoElfab)	1- Fluid mechanics Safety Relief Valves (PSV-*) 2- Rupture Discs (ORD-*) 3- Safety Heads / Rupture Disc Holders (PSE-*)	Protects the system from overpressure by safely relieving or isolating excess pressure, ensuring safe operation under HPHT conditions.
Pressure Control System (Provider: Equilibar)	Back Pressure Regulators (BPR-*)	Maintains stable back pressure; enables displacement of dead brine by live brine at the start of the test and provides controlled pressure during viscosity and density measurements.

In addition to the physical subsystems, the operation of the entire setup is coordinated through a centralized Control, Communication, and Data Acquisition System, which serves as the main platform for integrating all components and ensuring stable experimental operation. This system is based on a dedicated PC/workstation running PumpWorks software (Provider: AMETEK Chandler Engineering), which interfaces with all connected equipment, including pumps, sensors, separator, and fluid property measurement devices. It enables real-time interaction between hardware units, supports continuous monitoring and control, and ensures synchronized operation of all subsystems to maintain consistent experimental conditions throughout the steady-state CO_2–brine relative permeability measurements.
The system performs the following key functions:
Real-time data acquisition and logging:
Collects continuous measurements from sensors and equipment, including pressure transmitters (PTs), temperature sensors, densitometer, viscometer, and separator. Data is acquired in real time while being simultaneously recorded with accurate timestamps, stored reliably, and organized with metadata to enable secure export and post-processing/analysis.
System monitoring:
Provides real-time visualization of operating conditions such as pressure, flow rate, temperature, and fluid properties, allowing rapid detection of any instability.
Equipment control:
Enables direct control of high-pressure pumps (Quizix® QX-20000, Quizix® C-5000, Quizix® C-6000), including adjustment of flow rate, pressure levels, and operating modes.
Test procedure automation:
Supports execution of automated experimental sequences, including flow ramping, pressure stabilization, and scheduling of steady-state conditions.
Data logging and management:
Ensures reliable recording, storage, and export of experimental data for post-processing and analysis.

2.2.1 Pre-experimental conditioning of the HPHT setup for steady-state scCO₂–brine relative permeability testing

The closed-loop system, constructed with CO_2-compatible elastomers (AFLAS, FFKM) and Hastelloy

wetted parts, was cleaned via sequential solvent flushing. System integrity was verified using step-wise static and dynamic leakage tests with N_2 and DI water at target confining pressures prior to operation.

Determination of upstream and downstream dead volumes under closed-loop conditions

Prior to steady-state relative permeability measurements, the upstream and downstream dead volumes associated with the core holder system are determined. These volumes correspond to the internal void spaces within the flow lines, valves, fittings, pressure-transmitter connections, and core holder end plugs that are external to the core pore volume but contribute to fluid storage during operation. Their accurate estimation is required for reliable saturation calculations. In the present closed-loop configuration (as illustrated in **Fig. 1**):
Core upstream section (blue lines): from the injection system to the core inlet (including the fixed distribution plug), occupied by live brine.
Core downstream section (red lines): from the core outlet (including the floating distribution plug) to the separator, containing a two-phase mixture of live brine and CO_2.

The dead volumes are estimated geometrically using the known internal dimensions of all components. Volumes are incorporated into the total system volume during saturation calculations to ensure that only the core pore volume is considered. This improves the accuracy of the derived brine and gas relative permeability.

Absolute permeability measurement and dead brine displacement using live brine

Absolute permeability of the core is measured prior to the closed-loop steady-state relative permeability experiment using CO_2-saturated brine (live brine) under controlled flow conditions. In this step, the system is operated in an open-flow configuration, where live brine is injected into the core and the effluent is discharged through a back pressure regulator (BPR), without recirculation. This procedure serves two main purposes:
Absolute permeability measurement: Provides the single-phase permeability required for multiphase Darcy's law in relative permeability calculations.
Dead brine displacement: Replaces the initial dead brine with live brine, ensuring equilibrium fluid conditions before testing.

During this process, flow rate and pressure drop across the core are monitored until steady-state conditions are achieved. Based on these measurements, together with the core geometry and live brine viscosity, the absolute permeability of the core is determined using single-phase Darcy's law:

$$k = \frac{Q\mu L}{A\Delta P} \quad (1)$$

The absolute permeability calculation relied on the following measured parameters obtained under steady-state single-phase live-brine flow with outlet pressure controlled by the backpressure regulator: live-brine volumetric flow rate from the high-pressure syringe pump readout; differential pressure across the core from high-precision intelligent pressure transmitters; live-brine viscosity from prior HPHT viscometer measurements at experimental conditions; and core length and diameter measured with calipers, from which cross-sectional area was computed. These values were inserted into the single-phase form of Darcy's law to yield the Klinkenberg-corrected absolute permeability used as the reference for all subsequent relative permeability calculations.

2.2.2 Design of injection strategy and fractional flow schedule for steady-state relative permeability measurement

To ensure a strictly viscous-dominated flow regime, (where relative permeability becomes independent of flow rate and gravity override) total injection rates were scaled such that the macroscopic Capillary Number (N_{cv}) remained ≤10, following the established scaling criteria for heterogeneous CO_2–brine systems [39].

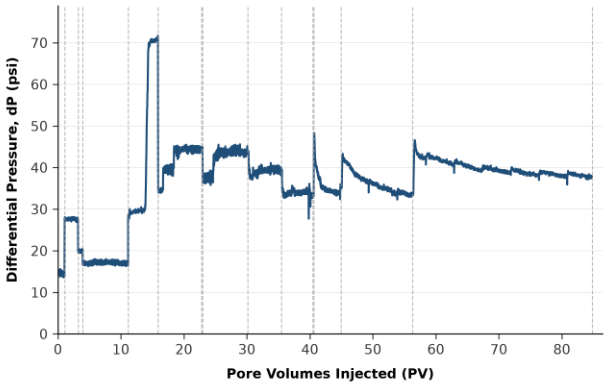

Fig. 2. Differential pressure across the core versus pore volumes injected over the primary-drainage fractional-flow and bump-rate sequence. The stable plateau reached within each step is the steady-state pressure drop used in the relative-permeability calculation.

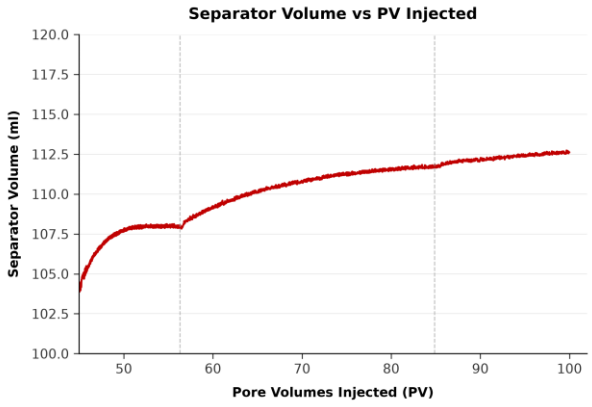

Fig. 3. Separator (produced-brine) volume versus pore volumes injected. The cumulative produced volume, with the system dead volumes, gives the average water saturation by material balance.

Concurrently, an upper limit must be enforced on these calculated flow rates to ensure they remain below the critical velocity threshold that would induce fines

migration or mechanical damage to the rock structure. This sequence is selected because:

It captures the principal saturation pathways during multiphase displacement,

It enables quantification of hysteresis between drainage and imbibition processes,

It provides reliable determination of key saturation endpoints, including minimum brine saturation ($S_{w,min}$) and residual gas saturation (S_{gr}), and

It allows assessment of data consistency and repeatability through a subsequent drainage cycle.

The injection schedule varies the fractional flow of CO_2 and brine in a stepwise manner while maintaining a nearly constant ΔP. Table 2 shows the complete sequence of steady-state steps, including bounding single-phase tare measurements and hysteresis cycles.

Table 2. Steady-state injection strategy and fractional flow schedule. The saturation reached at the end of each drainage step is the steady-state–established minimum water saturation ($S_{w,min} \approx S_{wi}$), which is generally higher than the true thermodynamic irreducible value (S_{wirr}); imbibition therefore begins from this steady-state $S_{w,min}$, and the secondary-drainage endpoint likewise denotes the steady-state $S_{w,min}$ rather than S_{wirr} (see Section 3.3).

Stage	Injection Strategy /Fractional Flow Trend	Initial Condition	Final Condition	Main Outcome and Purpose
Primary Drainage	Increase CO_2, decrease brine $f_{CO_2} \uparrow$ $f_w \downarrow$	Fully brine saturated	$S_{w,min}$	Establishes primary drainage relative permeability curves; defines gas mobility and identifies minimum brine saturation
Tare (Gas Phase)	Single-phase CO_2 (multi-rate) $f_{CO_2} = 1$ $f_w = 0$	End of drainage	—	Provides baseline gas flow behavior for data correction, validation of pressure–flow response, and consistency check
Primary Imbibition	Increase brine, decrease CO_2 $f_w \uparrow$ $f_{CO_2} \downarrow$	$S_{w,min}$	S_{gr}	Captures hysteresis between drainage and imbibition; quantifies residual gas saturation and brine re-saturation behavior
Tare (Brine Phase)	Single-phase brine (multi-rate) $f_w = 1$ $f_{CO_2} = 0$	End of imbibition	—	Provides baseline brine flow reference for correction of relative permeability data and verification of system response
Secondary Drainage	Increase CO_2, decrease brine $f_{CO_2} \uparrow$ $f_w \downarrow$	S_{gr}	Repeat $S_{w,min}$	Generates scanning curves; evaluates hysteresis effects, repeatability, and stability of wettability conditions

2.3 Methodology for core saturation and relative permeability determination in steady-state CO_2–brine systems

This section describes the methodology used to determine core saturation and relative permeability in steady-state CO_2–brine flow experiments. Core saturation is obtained using a material balance approach that tracks the distribution of brine within the closed-loop system. The calculation of relative permeability is based on a combination of measured and calculated parameters, including flow rates, pressure drop, fluid properties, and core properties, through Darcy-based relations. Together, these methods provide a consistent and reliable way to link the experimental measurements to relative permeability as a function of saturation.

2.3.1 Core saturation determination during drainage and imbibition

Core saturation is determined using a material balance approach based on the distribution of brine within the closed-loop system. This approach is applied during drainage, imbibition, and tare conditions at steady state.

At the start of the test, the relative permeability experiment begins with injection of live brine, and the system is fully saturated (fractional flow of brine $f_w = 1$). Under steady-state single-phase conditions, the total brine volume in the closed-loop system, $V_{\text{total, brine}}$, is defined. This volume includes the brine in the core, separator, and all external (dead) volumes, and serves as the reference for the material balance.

At each injection flow scenario during drainage and imbibition, once steady-state conditions are reached, the brine volume remaining in the core is determined from the following volume balance:

$$V_{\text{core,brine}}^{ss} = V_{\text{total brine}} - V_{\text{sep,brine}} - V_{\text{upstream}} - \left[(1 - f_{CO_2}) \times V_{\text{downstream}}\right] \quad (2)$$

where $V_{\text{sep,brine}}$ is the brine volume measured in the separator, V_{upstream} is the upstream dead volume fully occupied by brine, and $V_{\text{downstream}}$ is the downstream volume containing a two-phase mixture. The term $(1 - f_{CO_2})$ represents the brine fraction in the downstream section and ensures that only the brine contribution is included in the material balance. This formulation is valid for both drainage and imbibition processes.

The brine saturation in the core is then calculated as:

$$S_w = \frac{V^{ss}_{\text{core,brine}}}{PV_{\text{core}}} \quad (3)$$

2.3.2 Theoretical framework of steady-state multiphase flow in porous media

Phase relative permeabilities were calculated using the standard 1D steady-state multiphase Darcy equation, assuming uniform pressure gradients and constant fluid densities along the core. The calculated relative permeability values are then paired with the corresponding brine saturation obtained from the material balance approach described in previous sections. This allows the construction of relative permeability curves as a function of saturation, which describe the flow behavior of each phase within the porous medium.

2.3.3 Mitigation of capillary end effects via the modified intercept method (MIM)

To rigorously eliminate Capillary End Effect (CEE) artifacts without relying on expensive in-situ saturation monitoring (ISSM), this workflow applies the Modified Intercept Method (MIM). The approach builds upon the original Intercept Method introduced by Gupta and Maloney [14], which correctly identified that true relative permeability could be extracted from steady-state multi-rate tests at a constant fractional flow ($f_w = \frac{q_w}{q_w+q_{nw}}$). However, the original method relied on the assumption that the fractional length of the capillary-distorted region (L_{cee}/L) remained constant across varying flow rates. Goodarzian and Sorbie [32] demonstrated that this assumption is incorrect and established the Modified Intercept Method, proving mathematically that the CEE length (L_{cee}) is inversely proportional to the non-wetting phase flow rate (q_{nw}).

To execute the MIM, steady-state multi-rate tests ("bump tests") must be performed at each target fractional flow by incrementally increasing the total injection rate while keeping f_w constant. The true, artifact-free saturation and relative permeabilities are then extracted through a two-step linear extrapolation procedure:

Step 1: Determination of true saturation (S^*_w) At a constant fractional flow, the relationship between the average water saturation in the core ($\bar{S}_w$) and the reciprocal of the non-wetting phase flow rate ($1/q_{nw}$) is strictly linear. By plotting the experimentally measured $\bar{S}_w$ against $1/q_{nw}$ for the various bump rates (**Fig. 4a**), a straight line is established. Extrapolating this line to the y-intercept ($1/q_{nw} \to 0$) simulates an infinite flow rate where viscous forces entirely eclipse capillary retention, yielding the true, artifact-free saturation of the unaffected region (S^*_w).

Step 2: Determination of true relative permeability (k_{rnw} and k_{rw}) Similarly, plotting the total measured pressure drop of the non-wetting phase (ΔP_{nw}) versus q_{nw} forms a straight line (**Fig. 4b**). The slope of this line corresponds exactly to the viscous term $\frac{L\mu_{nw}}{kAk_{rnw}(S^*_w)}$. From this slope, the true, artifact-free non-wetting phase relative permeability (k_{rnw}) evaluated at S^*_w is directly calculated. Finally, the corresponding artifact-free wetting phase relative permeability (k_{rw}) is derived using the standard fractional flow ratio relationship evaluated at S^*_w.

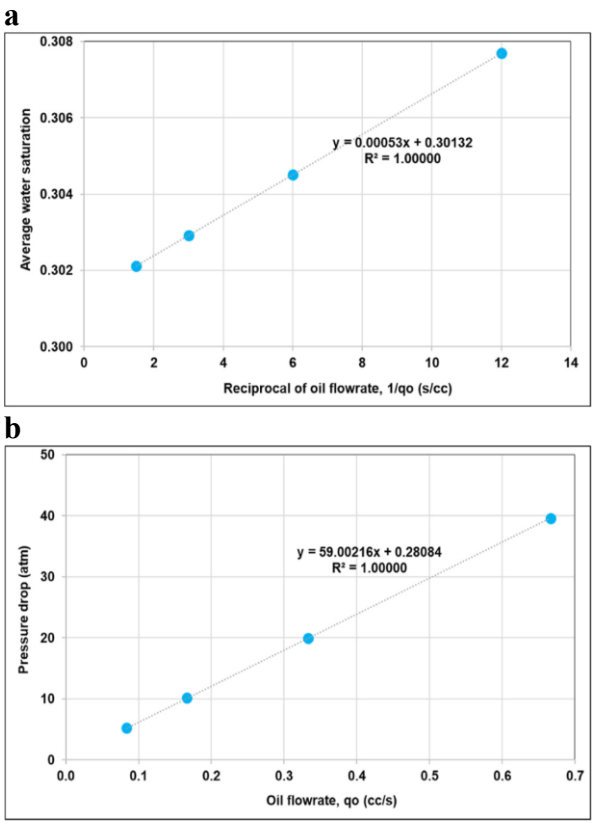

Fig. 4. Graphical implementation of the modified intercept method (MIM) for correcting capillary end effects during steady-state testing at a constant fractional flow. Panel (**a**) displays the measured average water saturation ($\bar{S}_w$) versus the reciprocal of the non-wetting phase flow rate ($1/q_{nw}$), where linear extrapolation to the y-intercept yields the true, artifact-free saturation (S^*_w). Panel (**b**) shows the total non-wetting phase pressure drop (ΔP_{nw}) versus the non-wetting phase flow rate (q_{nw}), where the slope of the linear regression is equal to $\frac{L\mu_{nw}}{kAk_{rnw}(S^*_w)}$, allowing for the direct extraction of the true phase mobility. Adapted from [32]. The original schematic in [32] uses oil as the non-wetting phase; here the modified intercept method is applied to a supercritical-CO_2–brine system.

2.4 Uncertainty analysis of saturation and relative permeability measurements

Accurate interpretation of steady-state CO_2–brine relative permeability measurements requires a rigorous quantification of experimental uncertainty. Brine saturation is obtained from a volumetric material balance of the closed-loop system. Using the previously defined formulation:

$$S_w = \frac{V_{total\,brine} - V_{sep,brine} - V_{upstream} - (1 - f_{CO_2})V_{downstream}}{PV_{core}} \quad (4)$$

Relative permeability is determined under steady-state conditions using the multiphase form of Darcy's law. For each phase, the effective permeability is calculated as:

$$k_\alpha = \frac{q_\alpha \, \mu_\alpha \, L}{A \, \Delta P} \quad (5)$$

and the corresponding relative permeability is obtained from:

$$k_{r\alpha} = \frac{k_\alpha}{k} \quad (6)$$

Uncertainty in brine saturation calculations, derived from material balance, was quantified through absolute propagation of errors from the following sources: the reference total system brine volume established at initial single-phase conditions; separator brine volume measurements from the acoustic level detection module; geometric uncertainties in upstream dead volume (brine-filled) and downstream two-phase volume; accuracy of CO_2 fractional flow settings from pump flow measurements; and uncertainty in core pore volume determined from gas porosity measurements.

Uncertainty in relative permeability was evaluated via absolute error propagation considering: phase flow rates (brine or CO_2) from pump accuracy specifications; phase viscosities from HPHT viscometer precision, with propagation through fluid property measurements; pressure drop across the core from pressure transducer accuracy; the independently measured absolute permeability; and core geometry (length and cross-sectional area) from caliper measurements. The resulting uncertainty bands were carried forward into the final reported kr curves to support simulator-ready data quality assessment.

2.5Post-experimental measurements and analysis following relative permeability testing

This section describes the measurements and analyses performed after completion of the relative permeability test. These steps are carried out to recover the remaining fluids, verify the volumetric balance of the system, and re-evaluate the core properties. The results provide a basis for validating the experimental data and assessing any changes in porosity and permeability caused by CO_2–brine flow under HPHT conditions.

2.5.1 Core depressurization (top blowdown) and mass balance verification

Following completion of the relative permeability experiment, the core was isolated and safely depressurized via a controlled top blowdown into an external condenser. A final volumetric mass balance was verified by confirming that the sum of the collected condenser brine, core-retained brine, and separator dead volumes matched the initial total system brine volume within experimental error, confirming system integrity and minimal fluid loss.

2.5.2 Post-Experimental core cleaning

Following testing and controlled depressurization, cores were dried and re-characterized for porosity and permeability. A final methanol flow-through cleaning cycle was used to distinguish between reversible fluid-retention effects and permanent structural/geochemical alterations to the pore network. Specifically, gas porosity and Klinkenberg-corrected permeability were measured before the experiment and again afterward, and the pre- and post-experiment values were compared as the quantitative indicator of any change in the pore network. Two post-experiment measurements were taken, one on the dried core and one after the methanol cleaning cycle, so that reversible fluid retention could be separated from permanent alteration.

3 Discussion

The workflow presented in this study directly addresses the persistent methodological and physical inconsistencies that have historically produced extreme scatter in steady-state $scCO_2$–brine relative permeability data. By consolidating a complete closed-loop HPHT architecture with rigorous quality-control gates at every stage, the methodology eliminates many of the artifacts (capillary end effects, transient mass transfer, drying-induced salt precipitation, and inadequate P–T stability) that undermine comparability across laboratories.

3.1 Critical quality-control elements for $scCO_2$–brine systems

The paired-test design and systematic evaluation of experimental stages reveal that four elements are particularly decisive for data reliability in low-viscosity, high-density $scCO_2$ systems. First, multi-day live-brine preparation and core equilibration are essential to suppress dissolution/exsolution transients and prevent artificial drying effects. Second, CO_2-specific seal-integrity hold tests (beyond standard N_2 screening) are required to detect slow leakage or permeation that would otherwise bias long-duration steady-state stages. Third, precise calibration of both line and separator dead volumes, combined with rigorous flash-handling protocols, ensures accurate separator-derived saturation trends. Finally, strict pressure–temperature control and differential-pressure tare/zero-offset correction are mandatory because even minor fluctuations in $scCO_2$ thermophysical properties can systematically distort relative permeability values. Together, these controls transform what has often been an ad-hoc process into a reproducible, artifact-minimized workflow.

3.2 The necessity of multi-rate checks and capillary end-effect mitigation

Capillary end effects remain a major source of bias in $scCO_2$–brine experiments owing to the exceptionally low viscosity of the non-wetting phase. The present study confirms that nominally identical fractional-flow steps

can produce rate-dependent saturations and underestimated CO_2 relative permeability unless multi-rate "bump" tests are performed and the Intercept Method is applied to extrapolate true mobility. These checks are therefore non-optional in best-practice steady-state work; they serve both as a diagnostic tool and as the basis for selecting an appropriate operating-rate window that minimizes end-effect distortion while remaining practical for laboratory timescales.

3.3 Translating experimental data to simulation-ready models

While the experimental workflow described above delivers high-quality, artifact-free steady-state data, raw laboratory relative permeability measurements are technically "scanning curves" rather than true bounding curves. Because flow-through experiments are limited by the pressure drop allowable to maintain fluid phase equilibrium, the core reaches a minimum water saturation ($S_{w,min}$) that is typically higher than the true thermodynamic irreducible water saturation (S_{wirr}) of the reservoir [33]. Inputting these raw scanning curves directly into a reservoir simulator artificially overestimates displacement efficiency and results in an underpredicted CO_2 plume size, which can negatively impact storage capacity estimates and monitoring plans [33]. Raw steady-state measurements produce scanning curves that terminate at the experimental minimum water saturation ($S_{w,min}$) rather than the true thermodynamic irreducible water saturation (S_{wirr}). To convert these into simulation-ready bounding curves, practitioners should extrapolate S_{wirr} and corresponding residual gas saturations using established analytical frameworks (e.g., Corey re-fitting and Land trapping correlations) as detailed in recent literature.

3.4 Recommendations for enhanced saturation verification

While the present workflow achieves accurate core-average saturation through high-precision acoustic separator measurements combined with rigorous dead-volume corrections and material balance, in-situ saturation monitoring (ISSM), such as medical X-ray computed tomography (CT) or nuclear magnetic resonance (NMR), is strongly recommended as a best-practice enhancement wherever available. These techniques provide independent, real-time visualization of saturation profiles along the core length, enabling direct confirmation of uniform saturation fronts, quantitative assessment of capillary end effects, and detection of local heterogeneity or gravity segregation that might not be apparent from separator data alone [1,11,18]. Laboratories equipped with ISSM capabilities are encouraged to integrate it as a complementary QC tool, particularly for heterogeneous or carbonate samples, to further increase confidence in the derived relative permeability curves.

3.5 History matching and the role of independent capillary-pressure and irreducible-saturation data

History matching of the full coreflood response provides an independent quality check on steady-state SCAL data. By reproducing the measured differential pressure together with the produced- and in-core-saturation history in a core-scale numerical simulator, the internal consistency of the experiment can be verified and the relative permeability and capillary-pressure (P_c) functions can be estimated jointly rather than separately; established tools that support this workflow include Sendra/S-Core (prores.no/solution/sendra), Core2Relperm (github.com/sede-open/Core2Relperm), CYDAR (Cydarex, cydarex.fr), and AutoScores (scores-panterra.nl) [35]. Although the modified intercept method removes capillary-end-effect artifacts from the relative permeability data, it does not by itself establish the true thermodynamic irreducible water saturation (S_{wirr}). The steady-state experiment terminates at a minimum water saturation ($S_{w,min}$) that is generally higher than S_{wirr} (Section 3.3). An independent capillary-pressure measurement (by porous plate or centrifuge) is therefore recommended to fix the initial water saturation, to anchor the bounding saturation functions, and to constrain the non-wetting endpoint $k_{r,scCO2}$ at S_{wirr}, which is otherwise sensitive to how S_{wirr} is defined [35,36,37]. Reporting $k_{r,scCO2}$ against an independently measured S_{wirr}, rather than against the experimental $S_{w,min}$, improves the transferability of the curves to field-scale CCUS simulation.

4 Conclusions

This work presents a complete, actionable best-practice workflow for generating high-quality, simulator-ready steady-state $scCO_2$–brine relative permeability data in a closed-loop HPHT system. By integrating rigorous controls across every stage, from core and fluid preparation, through system conditioning and leak-hold testing, fractional-flow design, multi-rate capillary end-effect mitigation (Intercept Method), simultaneous steady-state acceptance criteria (ΔP + flow rates + separator saturation trends), to absolute uncertainty propagation, the methodology directly addresses the unique experimental artifacts that have historically produced scatter in the $scCO_2$–brine k_r literature.

Key $scCO_2$-specific innovations include multi-day live-brine preparation and equilibration to eliminate mass-transfer and drying effects, CO_2-compatible materials and dedicated seal-integrity hold tests, precise geometric calibration of line and separator dead volumes, continuous P–T stability management with ΔP tare/zero-offset correction, and full hysteresis evaluation through drainage → imbibition → secondary drainage cycles.

Widespread adoption of these practices will improve reproducibility and the reliability of CCUS reservoir simulations. The full $scCO_2$–brine relative permeability datasets obtained with this workflow are reported in a companion paper (SCA2026-071).

This project is supported by the Hebron and Hibernia Projects and is managed by Energy Research & Innovation Newfoundland & Labrador (ERI). Any opinions, findings, and conclusions or recommendations expressed in this publication are those of the author(s) and do not necessarily reflect the views of the Hebron Project, Hibernia Project or ERI.
The authors are grateful to Lisa S. Lun (ExxonMobil Technology and Engineering Company), Daulet Magzymov (ExxonMobil Upstream Integrated Solutions Company), and John A. Molinaris (ExxonMobil Technology and Engineering Company) for their substantial intellectual input and constructive feedback provided during project meetings, which significantly strengthened this work.

References

1. S.C.M. Krevor, R. Pini, L. Zuo, S.M. Benson, Water Resour. Res. **48**, W02532 (2012)
2. T. Ajayi, J.S. Gomes, A. Bera, Pet. Sci. **16**, 1028 (2019)
3. N.M. Burnside, M. Naylor, Int. J. Greenh. Gas Control **23**, 1 (2014)
4. G.F. Teletzke, P. Lu, Energy Procedia **37**, 3936 (2013)
5. M.A. Hesse, F.M. Orr Jr., H.A. Tchelepi, Energy Procedia **1**, 3275 (2009)
6. C.H. Pentland, R. El-Maghraby, S. Iglauer, M.J. Blunt, Geophys. Res. Lett. **38**, L06401 (2011)
7. C.S. Land, Soc. Pet. Eng. J. **8**, 149 (1968)
8. E.J. Spiteri, R. Juanes, M.J. Blunt, F.M. Orr, SPE J. **13**, 277 (2008)
9. R. Juanes, E.J. Spiteri, F.M. Orr Jr., M.J. Blunt, Water Resour. Res. **42** (2006)
10. D.B. Bennion, S. Bachu, SPE Reserv. Eval. Eng. **11**, 487 (2008)
11. R. Pini, S.C.M. Krevor, S.M. Benson, Adv. Water Resour. **38**, 48 (2012)
12. C. Reynolds, M. Blunt, S. Krevor, Energy Procedia **63**, 5577 (2014)
13. X. Chen, A. Kianinejad, D.A. DiCarlo, Water Resour. Res. **52**, 8374 (2016)
14. R. Gupta, D.R. Maloney, SPE Reserv. Eval. Eng. **19**, 316 (2016)
15. S. Benson, *Carbon dioxide capture and storage in underground geologic formations* (2015)
16. G.A. Virnovsky, S.M. Skjaeveland, J. Surdal, P. Ingsøy, Steady-state relative permeability measurements corrected for capillary effects, Paper SPE 30541-MS presented at the SPE Annual Technical Conference and Exhibition, Dallas, Texas, 22–25 October 1995.
17. S. Richardson, B. Gao, E. Lyons, D. Magzymov, L. Poore, G. Besil, et al., Petrophysics **66**, 44 (2025)
18. M. Krause, J.-C. Perrin, S.M. Benson, SPE J. **16**, 768 (2011)
19. R. Miri, H. Hellevang, Int. J. Greenh. Gas Control **51**, 136 (2016)
20. E. Berrezueta, B. Ordóñez-Casado, L. Quintana, Solid Earth **7**, 37 (2016)
21. P. Berg, C. Moseley, J.O. Haerter, Nat. Geosci. **6**, 181 (2013)
22. M. Zettlitzer, F. Moeller, D. Morozova, P. Lokay, H. Würdemann, Int. J. Greenh. Gas Control **4**, 952 (2010)
23. H. Ott, K. de Kloe, F. Marcelis, A. Makurat, Energy Procedia **4**, 4425 (2011)
24. M. Mascle, S. Youssef, H. Deschamps, O. Vizika, Petrophysics **60**, 514 (2019)
25. L. Tang, G. Ding, S. Song, H. Wang, W. Xie, Y. Zhou, et al., Water **15** (2023)
26. A. Busch, N. Müller, Energy Procedia **4**, 6053 (2011)
27. N. Müller, Transp. Porous Media **87**, 367 (2011)
28. M.H. Krause, S.M. Benson, Adv. Water Resour. **83**, 376 (2015)
29. C. McPhee, J. Reed, I. Zubizarreta, *Core analysis: a best practice guide* (Elsevier, 2015)
30. B. Gao, L. Lun, R.C. Wattenbarger, SSRN 5010612 (2024)
31. M. Mascle, A. Oisel, P.K. Munkerud, E. Ebeltoft, O. Lopez, C. Pryme, et al., Petrophysics **66**, 26 (2025)
32. S. Goodarzian, K.S. Sorbie, Geoenergy Sci. Eng. **224**, 211626 (2023)
33. L.S. Lun, B. Gao, P. Krishnamurthy, K. Kohli, R.C. Wattenbarger, *ADIPEC*, SPE-216722-MS (2023)
34. Y. Guo, K. O. Vatne, 7th European IOR Symposium, Moscow, Russia (1993).
35. A. Sylte et al., Paper SCA2004-08, International Symposium of the Society of Core Analysts, Abu Dhabi, UAE (2004).
36. E. Ebeltoft et al., Petrophysics 66 (1) (2025).
37. J. G. Maas et al., Paper SCA2025-1037, International Symposium of the Society of Core Analysts, Hannover, Germany (2025).
38. T. Xu, J. A. Apps, K. Pruess, Chem. Geol. 217, 295 (2005).
39. C.-W. Kuo, S. M. Benson, Adv. Water Resour. 79, 1 (2015).